JGR Atmospheres

RESEARCH ARTICLE
10.1029/2022JD038374

Future Winter Precipitation Decreases Associated With the North Atlantic Warming Hole and Reduced Convection

Emilie C. Iversen[1,2], Øivind Hodnebrog[3], Lise Seland Graff[4], Bjørn Egil Nygaard[2], and Trond Iversen[1,4]

[1]University of Oslo, Oslo, Norway, [2]Kjeller Vindteknikk, Norconsult, Lillestrøm, Norway, [3]Center for International Climate Research (CICERO), Oslo, Norway, [4]Norwegian Meteorological Institute, Oslo, Norway

Key Points:

- Winter convective precipitation decreases by up to 50% toward the end of the century in the northeastern North Atlantic region
- This is associated with reduced sea surface temperatures (the North Atlantic warming hole), reduced evaporation and convection
- Future upstream shift in orographic precipitation distribution is likely affected by increasing static stability associated with the NAWH

Supporting Information:

Supporting Information may be found in the online version of this article.

Correspondence to:

E. C. Iversen,
emilie.claussen.iversen@norconsult.com

Citation:

Iversen, E. C., Hodnebrog, Ø., Seland Graff, L., Nygaard, B. E., & Iversen, T. (2023). Future winter precipitation decreases associated with the North Atlantic warming hole and reduced convection. *Journal of Geophysical Research: Atmospheres*, *128*, e2022JD038374. https://doi.org/10.1029/2022JD038374

Received 13 DEC 2022
Accepted 10 JUN 2023

Author Contributions:

Conceptualization: Emilie C. Iversen
Data curation: Emilie C. Iversen, Øivind Hodnebrog
Formal analysis: Emilie C. Iversen, Lise Seland Graff
Funding acquisition: Bjørn Egil Nygaard
Investigation: Emilie C. Iversen, Lise Seland Graff
Methodology: Emilie C. Iversen, Lise Seland Graff

Abstract Climate projections in the North Atlantic region suffer from great uncertainties, and projections of precipitation are given with a large spread. Some of this uncertainty is related to projections of the North Atlantic warming hole (NAWH). The Community Earth System Model version 2 (CESM2) projects a relatively strong and extensive NAWH, with future sea surface cooling extending to Northern Scandinavia. This study investigates the relatively large winter precipitation decrease projected by CESM2 in the northeastern North Atlantic region, reinforced in a regional model. Three future scenarios from CESM2 are dynamically downscaled with the Weather Research and Forecast model. A methodology to separate convective and orographic from stratiform precipitation is applied to explore the physical mechanisms. Changes in stratiform precipitation closely relate to storm-track changes, which varies between the scenarios. Convective precipitation decreases by up to 50% over the Norwegian Sea at the end of the century, which is robust across the scenarios. This is explained by the underlying reduced sea surface temperatures of the NAWH, leading to reduced evaporation and reduced convective activity and intensity. The orographic precipitation maximum over the Scandinavian mountains is shifted upstream, likely affected by increased static stability and flow blocking, which also relates to the NAWH. This shift is possibly also explained by more frequent rain versus snow, as well as reduced cross-barrier wind speeds. This study contributes to highlight the importance of focusing future research efforts on the NAWH, in order to constrain future climate projections in this region.

Plain Language Summary How precipitation patterns and amounts will change in the future is of high societal importance, for example, for hydropower, drinking water, irrigation, industry, and structural design. Given the large uncertainties involved in future climate projections this is still difficult to quantify. One uncertainty is related to climate model predictions of important ocean circulation features in the North Atlantic, which further affect projections of sea surface temperatures. The Community Earth System Model version 2 projects a large area of sea surface cooling in the North Atlantic toward the end of the century. In our study we point to possible connections between this cooling and future decreases in winter precipitation in the northeastern North Atlantic region. This is mostly associated with a reduction in convective precipitation, which is dependent on the temperature of the sea surface. In this area the Scandinavian mountains contribute significantly to the precipitation received through orographic effects. We also find a future upstream shift in the maxima of orographic precipitation, which is indicated to be also (partly) connected to the sea surface cooling. These findings may help in understanding the large spread in future precipitation projections in this region and should urge for more research toward constraining them.

1. Introduction

Climate projections in the North Atlantic region suffer from great uncertainties. Part of this relates to the large natural climate variability of the region, which is difficult to distinguish from an anthropogenic warming signal, for example, the North Atlantic Oscillation and associated variability in the storm tracks and jet stream. Uncertainties are also related to a thug-of-war between the dynamical responses to non-uniform warming of the region, for example, Arctic Amplification versus upper-tropospheric tropical warming (Oudar et al., 2020; Screen et al., 2018; Shaw et al., 2016; Zappa & Shepherd, 2017), as well as model representations of important ocean circulation features and the sea surface temperature (SST) gradients they produce (Bellomo et al., 2021; Cohen et al., 2020; Gervais et al., 2019; Nakamura et al., 2004). Precipitation is a variable greatly affected by this uncertainty. Projections of precipitation by general circulation models (GCMs) also suffer from the drawbacks connected with parameterizations of sub-grid convection (Hohenegger et al., 2008; Kendon et al., 2020;

Project Administration: Emilie C. Iversen, Bjørn Egil Nygaard
Resources: Øivind Hodnebrog
Software: Emilie C. Iversen, Lise Seland Graff
Supervision: Bjørn Egil Nygaard, Trond Iversen
Validation: Emilie C. Iversen
Visualization: Emilie C. Iversen, Øivind Hodnebrog, Lise Seland Graff
Writing – original draft: Emilie C. Iversen
Writing – review & editing: Emilie C. Iversen, Øivind Hodnebrog, Lise Seland Graff, Trond Iversen

Li et al., 2019; Prein et al., 2015; Tang et al., 2021; Tomassini et al., 2017; Trenberth et al., 2003; Wilcox & Donner, 2007), as well as being too coarse to resolve regional detail. Future changes in precipitation have substantial consequences for society at a regional and local scale, for example, for hydropower generation, water consumption, irrigation, industry, and infrastructure design. Winter precipitation is of particular importance as snowpacks acts as natural reservoirs, and occurrence of icing on structures can cause major damage (Barnett et al., 2008; Iversen et al., 2023). It is thereby essential to better understand the physical mechanisms of the precipitation responses at this scale, to better constrain climate model projections (Trenberth et al., 2003).

Part of the uncertainty in North Atlantic climate projections relates to a phenomenon termed the North Atlantic Warming Hole (NAWH). The NAWH is an area within the North Atlantic subpolar gyre with a striking deficit in surface warming, which has been linked to a slowdown of the Atlantic Meridional Overturning Circulation (AMOC) (Drijfhout et al., 2012; Keil et al., 2020; Liu et al., 2020). In future projections, SST gradients associated with SST anomalies in the North Atlantic cause an increase in the meridional surface temperature gradient between the subpolar and subtropical gyre, leading to increased baroclinicity, and the potential for enhanced storm activity over the North Atlantic and Europe (Gervais et al., 2019; Hand et al., 2019; Inatsu et al., 2003; Nakamura et al., 2004; Wilson et al., 2009; Woollings, Gregory, et al., 2012). The jet and storm tracks have been shown to be sensitive to the location of SST gradients relative to the mean jet position in models of varying complexity (Brayshaw et al., 2008; Gervais et al., 2019; Graff & LaCasce, 2012; Nakamura et al., 2004). Consequently, the NAWH depth, spatial extent and location in climate models play a crucial role in their projections of North Atlantic climate (Bellomo et al., 2021).

The AMOC slowdown/NAWH has been associated with a precipitation decrease in the North Atlantic region (Bellomo et al., 2021; Liu et al., 2020). The NAWH impacts precipitation through its impacts on the jet stream and storm tracks, as well as the surface heat fluxes (Gervais et al., 2020). In sensitivity experiments with the Community Earth System Model (CESM) where they isolated the effects of the NAWH, Gervais et al. (2020) found precipitation to be suppressed directly over the NAWH. This was mostly influenced by the direct effect of lowered SST and turbulent heat fluxes. Hand et al. (2019) also performed sensitivity experiments, using the Max Plank Institute for Meteorology Earth System Model (MPI-ESM), and showed that precipitation suppression in conjunction with the NAWH was apparent when local SST pattern changes were isolated, while precipitation increased in the same region when all global warming related aspects were included (including increased storminess). Using the Met Office Hadley Centre's GCM, HadGEM3, Jackson et al. (2015) found less precipitation and evaporation over Europe and the North Atlantic and strengthened storm tracks. Woollings, Harvey, et al. (2012) highlighted the connection between increased atmospheric static stability and the NAWH, as the warming at upper levels are stronger than at the surface. Increased static stability was also shown in Hand et al. (2019).

At a regional and local scale, stratiform, convective and orographic precipitation (in mountainous regions) contribute to the total precipitation received, and these are produced by different physical mechanisms (Houze, 2014). While previous studies have considered changes in projected winter precipitation in the North Atlantic region in relation to the NAWH (Gervais et al., 2020; Hand et al., 2019; Jackson et al., 2015; Swingedouw et al., 2021), this has not been related directly to the different precipitation types. As was highlighted by for example, Hand et al. (2014) and Lebeaupin et al. (2006), stratiform and convective precipitation respond differently to changes in underlying SSTs, and orographic flow theory explains how orographic precipitation is strongly influenced by static stability (Kirshbaum et al., 2018; Smith, 1989). To fully understand the precipitation responses and associated uncertainties in this region, these precipitation types should be investigated separately. Given the large errors associated with convection schemes of global models, as well as the relatively coarse resolution and poorly resolved orography, a higher resolution model without parameterized convection should be applied for this purpose (Kendon et al., 2020; Vergara-Temprado et al., 2020).

Motivated by a discovered relatively large winter precipitation decrease in Iversen et al. (2023), based on three future scenarios from the CESM version 2 (CESM2) (Danabasoglu et al., 2020) downscaled with the Weather Research and Forecasting (WRF) model (Skamarock et al., 2019), we here further explore these data to investigate the physical mechanisms behind this precipitation response. It was hypothesized that the relatively strong and extensive NAWH in CESM2 (as compared to other CMIP6 models) is largely contributing to this response. The WRF data is on a 12 km grid and has explicit treatment of convection, covering an area in the northeastern North Atlantic region. We investigate changes in stratiform, convective and orographic precipitation, with a specific focus on the influences of the NAWH. Changes to orographic precipitation are investigated over the

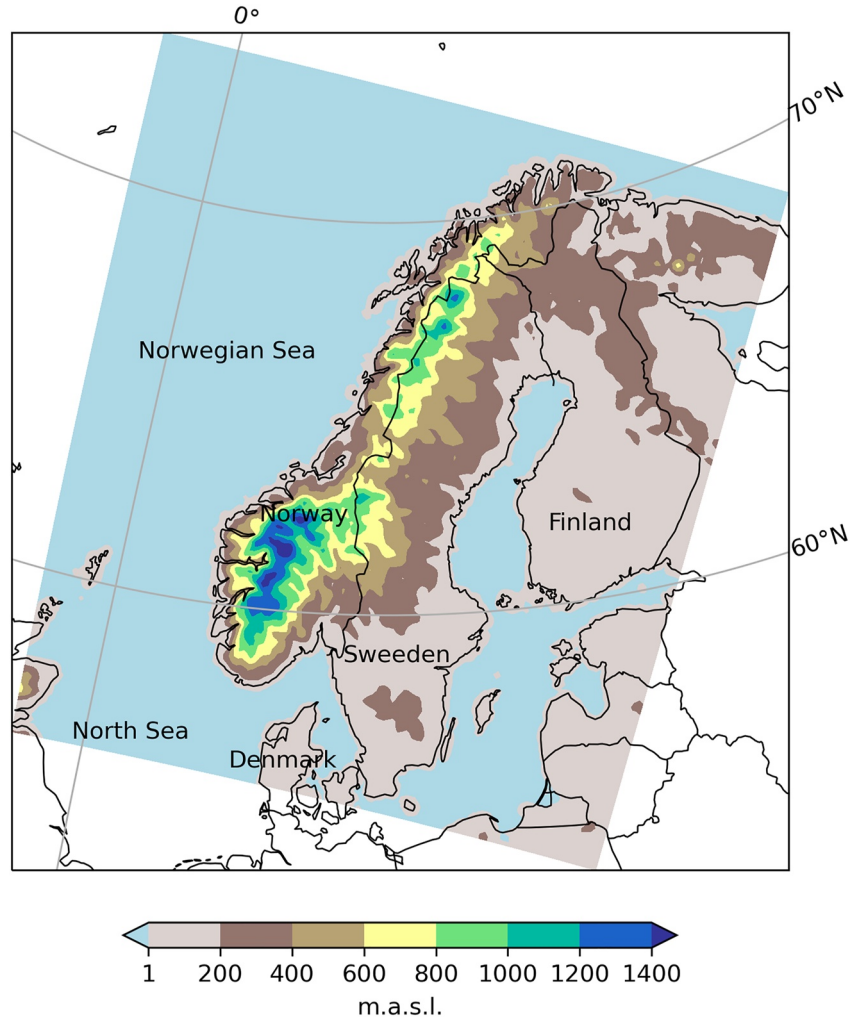

Figure 1. Spatial extent and terrain height (m above sea level) of the WRF domain.

Scandinavian mountains, as this precipitation type contributes considerably to the precipitation received in this region. We focus on the December-February (DJF) winter season, when SST impacts on precipitation generation in the region is strong. The study does not seek to quantify potential future precipitation changes, but rather to highlight physical mechanisms of climate change responses, with a specific focus on the impacts of projected SST anomalies in the North Atlantic, to better understand the reasons behind the large spread in climate model projections in the region. The paper is structured as follows: Data and methods are presented in Section 2, results in Section 3, discussion in Section 4 and summary and conclusions in Section 5.

2. Data and Methods

2.1. Regional Model Configuration and Downscaling

The WRF model (version 4.1.2) is set up with one domain with a horizontal grid spacing of 12 km and 32 vertical levels (the upper level is at 100 hPa and the level density decreases with height). The domain covers Scandinavia, the Norwegian Sea and the North Sea (Figure 1). The temporal resolution of the data is 1 hr. Parameterization scheme choices are listed in Table 1. The chosen grid spacing is within the "convective gray zone," yet no parameterization of convection is used due to indications of better model performance with explicitly treated rather than parameterized convection up to around 25 km grid spacing (Birch et al., 2015; Dirmeyer et al., 2012; Field et al., 2017; Hohenegger et al., 2015; Pearson et al., 2014; Stein et al., 2015; Vellinga et al., 2016; Vergara-Temprado et al., 2020). Kendon et al. (2020) highlight the inability of convective parameterizations to advect convection due to their lack of memory, relevant for typical winter conditions in this region where ocean

Table 1
Parameterization Scheme Choices for the WRF Model Configuration

Type of scheme	Name	References
Microphysics	Thompson-Eidhammer aerosol-aware (with mod. regarding melting snow)	Thompson and Eidhammer (2014) Iversen et al. (2021)
Boundary layer	Mellor-Yamada-Nakanishi-Niino 2 (MYNN2)	Nakanishi and Niino (2006)
Radiation	Rapid radiative transfer model for GCMs (RRTMG)	Iacono et al. (2008)
Land surface	Noah	Mitchell (2005)

triggered convection is advected over land. The choice of 12 km grid spacing is a compromise between accuracy and computational requirements, and enables near century-long simulations with three emission scenarios, needed to evaluate robustness in the regional model responses.

Boundary conditions were updated in WRF every 6 hr and spectral nudging was applied for temperature, horizontal winds and geopotential height. Sea-surface temperatures were updated daily in WRF from the CESM2 data.

Three future scenarios from CESM2 have been downscaled: ssp126 (a sustainable future), ssp245 (middle of the road) and ssp370 (more pessimistic development trends) (O'Neill et al., 2016), and the ensemble member "r11" (due to being the only member with all necessary fields for downscaling with WRF available at the time). The primary focus of this study will be on ssp370 and the future period 2080–2100, relative to 2015–2035, when the forcing is strongest, while the other scenarios will be shown in Supporting Information S1. The model and data is described in more detail in Iversen et al. (2023).

2.2. Precipitation Type Separation

Stratiform, convective and orographic precipitation are referred to as precipitation types through this paper. To separate out the convective component of precipitation, the method of Poujol et al. (2020) is adopted with some modifications. The method is based on detecting the overturning circulation of convection, by utilizing the standard deviation of vertical velocity at 500 hPa. Due to the vast amount of data generated by our simulations, and the original purpose of application for atmospheric ground icing, only the 10 lowest vertical levels of the model were saved (roughly the boundary layer). Hence, the detection of up- and downdrafts in our data is performed at the highest model level (roughly 700–800 hPa). Given that winter convection over the Norwegian Sea is relatively shallow, this level showed to be sufficient for detecting the convective overturning.

Vertical velocity is significantly affected by topography, and so in Poujol et al. (2020) convection was identified above terrain through potential vorticity dipoles and uplift vertical velocity at necessary levels of the atmosphere not available in our data. Here we assume that the precipitation type occurring over topography (west of the topographic barrier only) is the same as over the Norwegian Sea at a given time (assuming westerly advection; Figure S1 in Supporting Information S1 shows that close to all of the precipitation received west of the topographic barrier is advected by westerly winds. See Supporting Information S1 for more details on this methodology). Precipitation east of the topographic barrier is not as highly correlated with westerly flow and hence cannot be classified. If the precipitation only occurs over land at a given time, it is characterized as orographic, assuming it is generated by orographic lifting of moist air. The precipitation not classified as either convective or orographic is classified as stratiform. Orographically enhanced stratiform precipitation is therefore also classified as such.

A validation of this algorithm is not carried out, however a comprehensive visual inspection confirms its qualitative validity (Figure S2 in Supporting Information S1 shows two example cases of the performance).

3. Results

While the main focus of this paper is on the downscaled results, we first consider some key fields directly from the global model in order to compare with and highlight the benefits of the regional model.

3.1. Global Model

The projected warming hole in CESM2 is one of the strongest and most extensive among the CMIP6 models (Figure S3 in Supporting Information S1), with cooling reaching as far northeast as Norway (Figure 2a). Seasonal

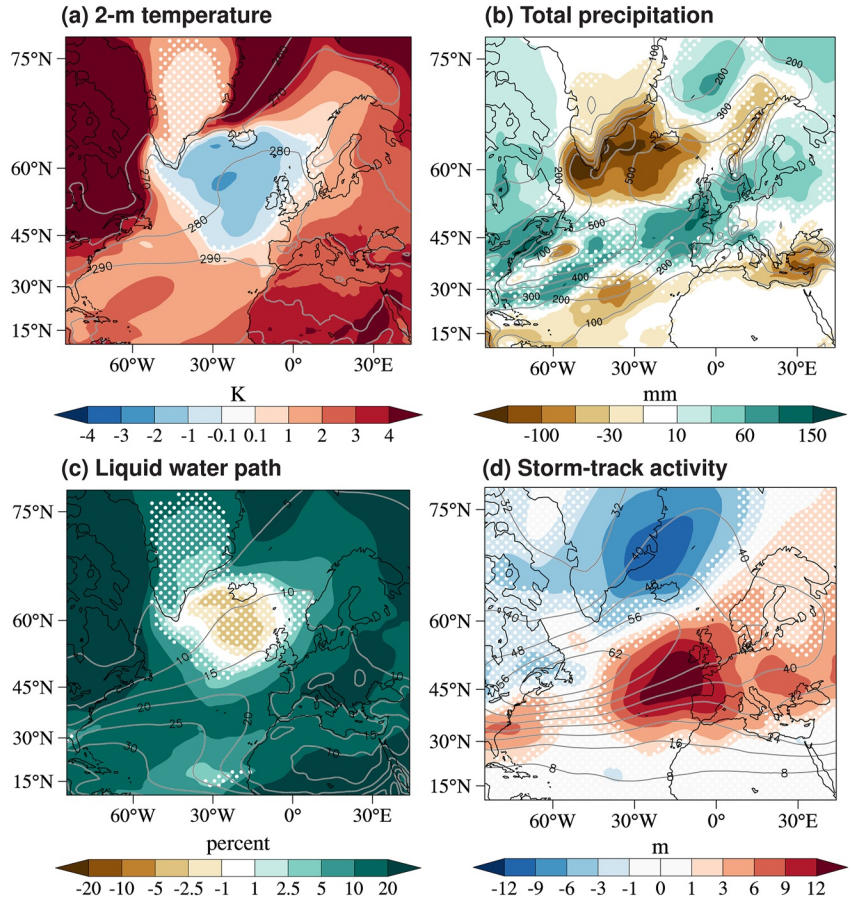

Figure 2. Change fields from CESM2 ssp370 member r11, between 2015–2035 and 2080–2100 for the winter season (DJF). Contours display the reference period mean (2015–2035). Note that the contour values for liquid water path in (c) is kg/kg. Storm-track activity is in terms of standard deviation of bandpass-filtered geopotential height at 500 hPa (see Supporting Information S1 for details). White dots indicate non-significant changes at the 5% level according to the Welch *t*-test.

total accumulated precipitation (Figure 2b) and mean liquid water path (LWP) (Figure 2c) is decreasing directly above the NAWH, and precipitation is also decreasing over an area covering most of the Norwegian Sea. This is a robust response in CESM2, seen in the ensemble mean of ssp370, as well as ssp126 and ssp245 (Figures S4–S6 in Supporting Information S1). Storm-track changes vary more between the scenarios. Changes are largest for ssp370, with increased storm activity over large parts of Europe (including Norway, however non-significant in the ensemble member used for downscaling), and reduced activity over the Greenland Sea (Figure 2d and Figure S6 in Supporting Information S1). In ssp126 the maximum storm activity increase is located further north, over the British Isles and the North Sea, and activity is increasing over the entire Norwegian Sea (significantly only south of ~69°N) (Figure S4 in Supporting Information S1). The changes in ssp245 are similar to ssp370 but weaker (Figure S5 in Supporting Information S1).

3.2. Regional Model

By using a regional model (WRF) with 12 km grid spacing, the winter precipitation over most of the Norwegian Sea is increased by 20%–30% compared to CESM2, and over the Scandinavian Mountains by roughly 60%, as orographic precipitation enhancement is better captured (Figure 3). North of 70°N WRF produces up to 100% more precipitation. WRF produces substantially more convective precipitation (P_c) than CESM2, both in terms of fraction of total precipitation and absolute values (Figure 3, bottom). In the area north of 70°N, WRF P_c fraction peaks at 0.6 (equaling 300–400 mm), while the CESM2 fraction is 0.1 (equaling 10–100 mm). This area is associated with polar lows which are of too small scale (~200–1,000 km) to be fully resolved by most present-day GCMs (Kolstad & Bracegirdle, 2008; Kolstad et al., 2009; Landgren et al., 2019). This is also a favorable area for

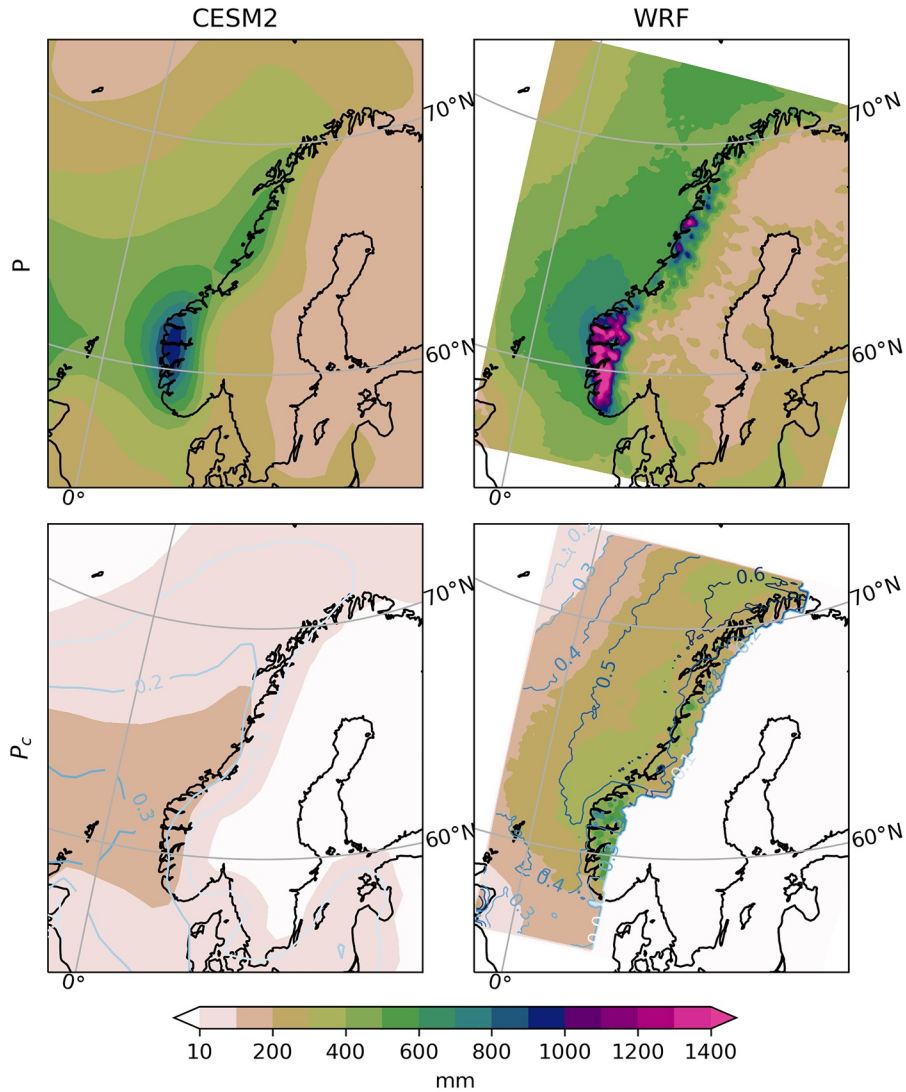

Figure 3. Comparison of winter (DJF) mean CESM2 (left) and WRF (right) total precipitation (top) and convective precipitation (bottom), from the period 2015–2035. Contours in the bottom panels display the fraction of total precipitation. (WRF convective precipitation could not be identified east of the Norwegian topographic barrier, see Section 2.2).

marine cold air outbreaks (MCAOs) and associated convection, which in CESM2 relies strongly on parameterized, subgrid-scale processes, while in WRF relies on explicit treatment on a 12 km grid scale. Given that Field et al. (2017) demonstrated that accumulated precipitation from MCAO event show relatively small differences between simulations with and without a convection scheme for similar grid scales in this region, it is reasonable to think that WRF with its higher resolution improves the representation of winter total P and P_c here.

Figure 4 shows future changes in WRF variables. The future surface temperature (T_s) change includes a cooling that extends northwards along the Norwegian coastline (maximum 2°C within the domain) (Figure 4a). Over the northerly corners of the domain the sea is ice covered in the reference period while mostly ice free in the future period, causing a T_s warming here. Precipitation (P) decreases over the Norwegian Sea (50–200 mm, 10%–30%) and the Scandinavian Mountains (more than 200 mm, ∼30%) (Figure 4b). P increases over the southern North Sea (up to 100 mm, ∼10%), over the sea-ice melting northerly corners, and over most of the remaining land masses. This change signal is similar to CESM2 in terms of percent, but larger in terms of absolute values, and CESM2 lacks the orographic component (Figure 2b).

Figures 4c and 4d show how changes in atmospheric static stability (here calculated simply as the difference between temperature at 700 hPa (T_{700}) and at the surface (T_s)) and evaporation (E) closely follow the change in

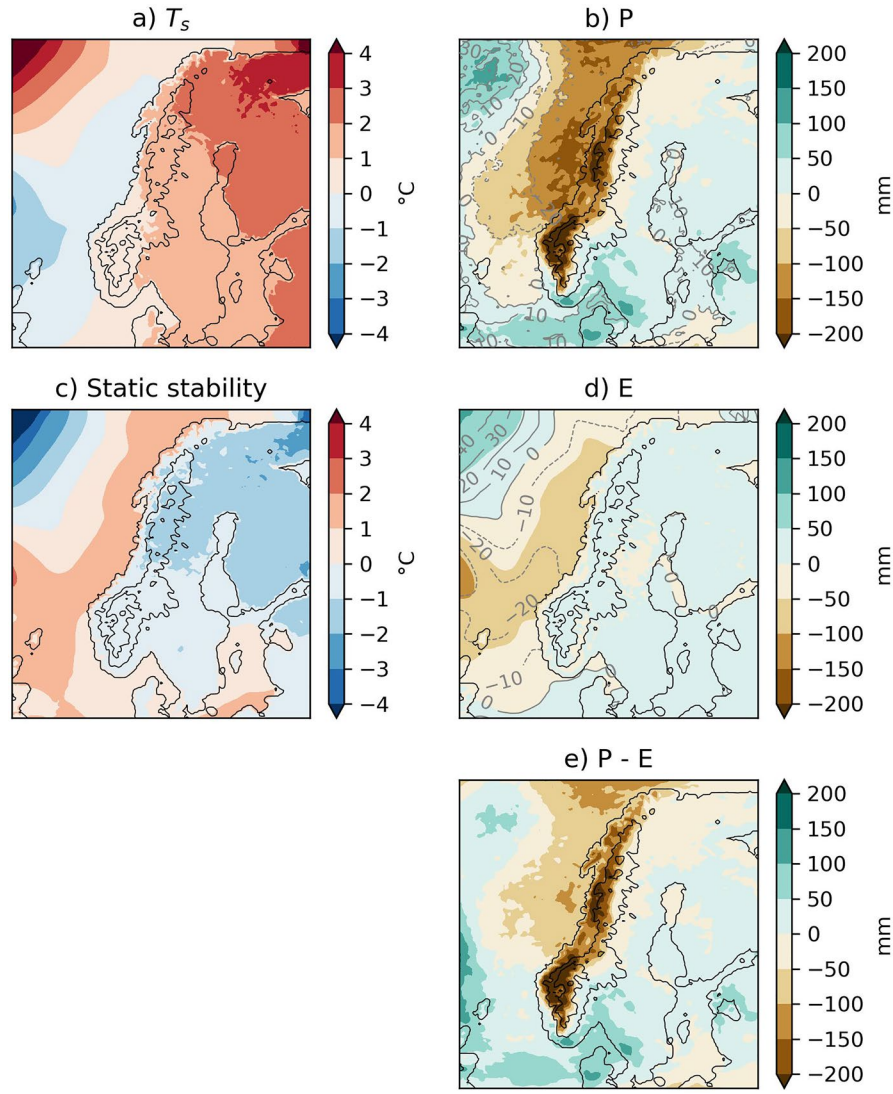

Figure 4. Change in WRF winter (DJF) (a) mean surface temperature (T_s), (b) total precipitation (P), (c) mean static stability (T_{700}-T_s), (d) total evaporation (E), and (e) P–E, between 2015–2035 and 2080–2100 (ssp370). Gray contours in panels (b) and (d) present the relative change (in %) (not shown above terrain). Black height contours are given for 500 m intervals.

T_s. Static stability is increasing over the Norwegian Sea, North Sea, and Baltic Sea where the ocean surface cools, as the upper troposphere is warming (Woollings, Harvey, et al., 2012). E decreases alongside T_s, by 50–100 mm (10%–30%) for large parts of the Norwegian Sea (E increases over the northerly corners as sea ice is melting). The change in P minus E (Figure 4e) reflects the changes to P brought upon by changes in horizontal moisture transport (Trenberth, 1999), and indicates decreased moisture transport into the northern half of the domain (except for the northwest corner where sea ice is melting), and increased transport into the southern half. This further indicates that the decrease in E over the southern part of the Norwegian Sea dominates the increased moisture transport and causes reduced P.

Results from the separation of stratiform, convective and orographic precipitation (P_s, P_c, and P_o respectively) are shown in Figure 5 (as winter totals). Reference period (2015–2035) P_s is occurring relatively evenly across the ocean, with a maximum over West Norway (300–400 mm), and has an orographic component over the mountains reaching 1,000 mm (Figure 5b). Its fractional contribution to the total precipitation is largest to the south over the North Sea and over the ice-covered northwest corner (>0.6), and smallest over North Norway (<0.4). With future warming, P_s is decreasing by 10%–40% north of and increasing by 10%–30% south of about 65°N (mid-domain) over the ocean (Figure 5f). Where P_s is increasing, its frequency is also increasing, however the

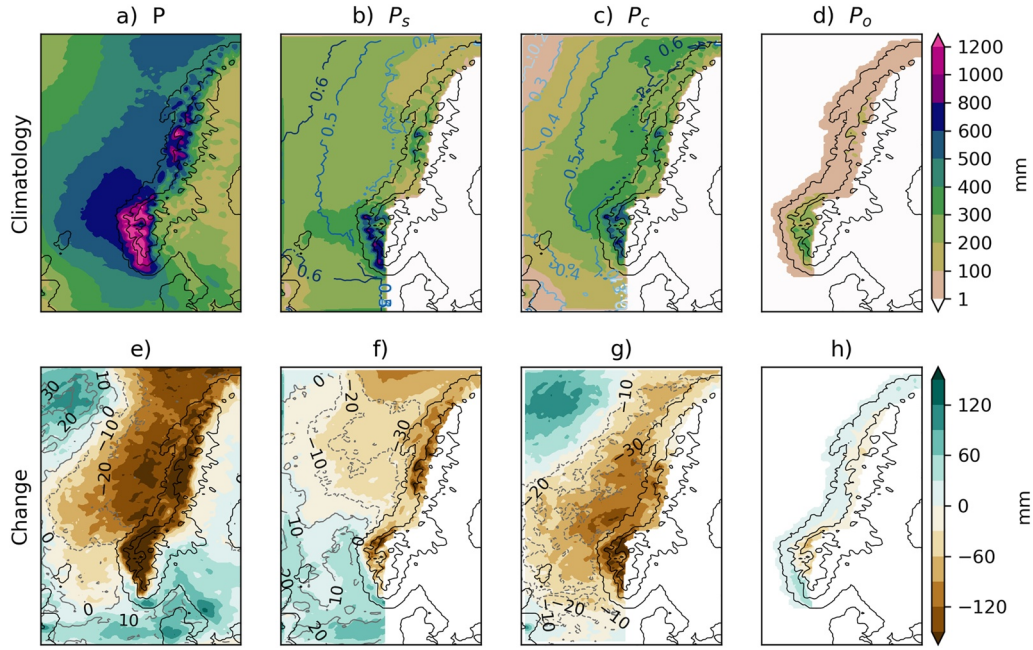

Figure 5. WRF reference period (2015–2035) total winter (DJF) precipitation (P; a) and its stratiform (P_s; b), convective (P_c; c) and pure orographic (P_o; d) components, and the future change (2080–2100) (ssp370) (e, f, g, h, respectively). Contours in the top panels (b, c) display the fraction of total precipitation. Contours in the bottom panels (e, f, g) display percentage change (Contours are not shown over topography, and hence not for P_o, due to disturbance from height contours). Significance of the changes were tested using a Mann Whitney U-test and yielded significant changes (at the 5% level) for all areas, except for the narrow zones with small values between increasing and decreasing changes, and is not shown. (The precipitation types could not be identified east of the Norwegian topographic barrier, see Section 2.2).

amount increases more than the frequency due to a larger fractional increase in the highest intensities (Figure S7 in Supporting Information S1). P_s in this region is predominantly associated with fronts of low-pressure systems, whose moisture to a large degree originates from sources further away from the sink region (Catto et al., 2012; Lavers & Villarini, 2013; Stohl et al., 2008; Trenberth, 1999). The P_s changes are in good agreement with the storm-track changes of the global model (Figure 2d), and reflects the contribution from changes in horizontal moisture transport to changes in P in the domain (compare Figures 4e and 5f).

In WRF, dominant wind directions along Norway are rotated from westerly toward southwesterly/southerly in the future climate (Figure S8 in Supporting Information S1), indicating a higher frequency of storm tracks with a more southwest–northeast oriented path toward Scandinavia. On this path, the storms pass across a warmer ocean surface than they would coming more from the west across the NAWH, and hence pick up more moisture along the way. This is supported by the CESM2 horizontal moisture flux across WRF's boundaries, which decreases along the western and increases along the southern boundary (Figure S9 in Supporting Information S1) (consistent with the change in LWP in Figure 2c), which supports the increased P_s intensity to the south in the domain. A similar anomalous southwesterly flow was also found in a couple of the sensitivity experiments of Gervais et al. (2020).

The reference period P_c shows a favorable area of occurrence (Figure 5c). The largest P_c values and fractions are found over the Norwegian Sea closest to the Norwegian coastline (200–400 mm, fraction of 0.5–0.6), and the maximum fraction (>0.6) is located further north (convection rarely occurs over the northwest corner due to sea ice). This corresponds to typical areas for cold air advection behind passing low-pressure systems and marine cold air outbreaks (MCAO) (Kolstad et al., 2009; Landgren et al., 2019; Papritz & Grams, 2018). These provide ideal conditions for convection, as the colder air above the warmer ocean surface creates instability and exchange of latent heat (Brümmer, 1997, 1999; Papritz & Spengler, 2017).

Future WRF P_c decreases over the favorable area of occurrence, with the largest decrease occurring over the reference period maximum (as much as 150 mm, >30%) (P_c is increasing in the northwest corner as sea ice is melting

and leaving an open ocean surface) (Figure 5g). The reduction corresponds to a 30% decrease in frequency (Figure S10 in Supporting Information S1). All convective precipitation intensities are decreasing, more so for higher intensities. In the cold, dense air masses above the Norwegian Sea, the convection is typically relatively shallow with surface-layer-based updrafts (Kendon et al., 2020), and generated precipitation is largely associated with local moisture sources from evaporation (Papritz & Sodemann, 2018). Consequently, the decrease in convective precipitation is well explained by the decrease in SST, T_s, evaporation and static stability (Figure 4).

As is expected, the reference period P_o shows a positive gradient from low to high terrain (Figure 5d). P_o shows a distinct change pattern of increase for terrain below roughly 500 m.a.s.l. (10%–50%) and decrease above (10%–30%) (Figure 5h). This pattern is also evident for P_s over southern Norway (Figure 3f), where there is orographic enhancement of P_s. Given that close to all precipitation received on these western mountain slopes in winter is carried with westerly winds (180–345°, Figure S1 in Supporting Information S1), this implies an upstream shift in the geographic distribution of P_o. The dynamical response of the impinging moist flow depends on the nondimensional mountain height ($M = Nh_m/U$), where N is the mean Brunt- Väisälä frequency, h_m the crest height and U the mean cross-barrier wind speed (Smith, 1989). Larger M reflects stronger terrain blocking, more flow deflection, reduced vertical lift, and upstream shifted P_o maximum (Colle, 2004). We therefore hypothesize that the P_o change is partly due to the increased static stability (increasing N) and rotation of prevailing wind direction (Figure S8 in Supporting Information S1) (reducing U). The change might also be partly caused by a shift from frozen to liquid precipitation with warming. Rain has a higher fall velocity than snow and so is horizontally advected a shorter distance before reaching the ground, hence also contributing to shift the precipitation maxima upstream (Pavelsky et al., 2012).

Indications to support these hypotheses can be seen in the vertical cross sections in Figure 6. The Brunt-Väisälä frequency squared (N^2) is mostly increasing and vertical velocity (W) is decreasing over the windward slope, particularly the upper portion. The reduced orographically induced cloud water (QCLOUD) at the upper slope and graupel (QGRAUP) over the whole windward slope might be connected to the reduced vertical lift. Isolation of westerly wind directions reveals that U is decreasing (at all levels, not shown), indicating that westerly wind speeds are reduced in addition to being less frequent. All these factors support increasing M. Also evident is an increase in rain (QRAIN) over the whole windward slope, with a maximum at the foot of the mountain, and decrease in snow (QSNOW) over the upper slope and crest. This may indicate that the warming present over the windward slope increases the melting level and the vertical depth of rain above ground at the expense of snow.

The precipitation type separation was also performed for the ssp126 and ssp245 downscaled simulations, with very similar results, and hence is not shown.

4. Discussion

Most studies that investigate future changes in precipitation types (convective, stratiform, and orographic) find increased convective precipitation in both summer and winter, typically at higher rates than stratiform, as the climate warms (Berg et al., 2013; Chernokulsky et al., 2019; Han et al., 2016; Hand et al., 2014; Kendon et al., 2020; Poujol et al., 2021; Rulfová & Kyselý, 2013). The high sensitivity of convective precipitation to surface temperature changes is confirmed here, however, with the opposite sign to most other studies due to the decreased surface temperatures of the NAWH in our model. Poujol et al. (2021) and Kendon et al. (2020) studied precipitation type changes in our region of interest, but are based on input from single global models or ensemble means where the NAWH is significantly less pronounced than in CESM2. Our results are however in agreement with several other studies; Lepore et al. (2021) showed reduced convective available potential energy (CAPE) over the NAWH in a CMIP6 model ensemble. Landgren et al. (2019) found decreases in MCAOs in the region due to the increased static stability, based on the CESM large ensemble (Kay et al., 2015). Also related are the findings of reduced polar low activity in the northern seas linked to the increased stability (Bresson et al., 2022; Mallet et al., 2017; Woollings, Harvey, et al., 2012; Zahn & von Storch, 2010).

As for the change in orographic precipitation, our results are consistent with the literature (Colle, 2004) regarding increased static stability and flow blocking (Hughes et al., 2009; Kirshbaum & Smith, 2008; Panziera & Germann, 2010; Purnell & Kirshbaum, 2018), reduced cross-barrier wind speed (Luce et al., 2013; Panziera & Germann, 2010; Smith & Barstad, 2004), and precipitation phase shift (Pavelsky et al., 2012). Other research has pointed to mechanisms related to changes in thermodynamics and microphysics with warming, such as the level

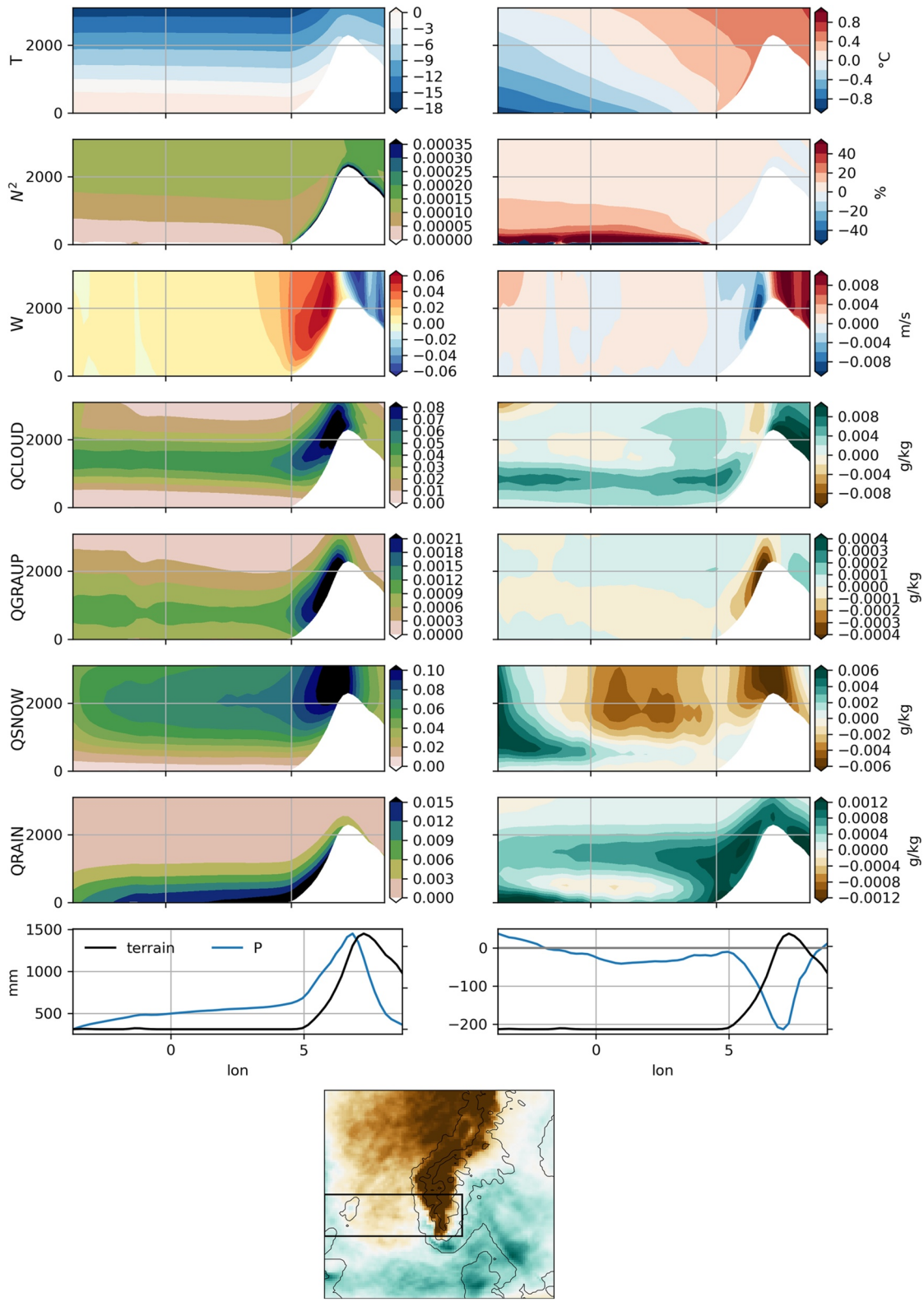

Figure 6. Vertical cross sections of WRF winter (DJF) mean temperature (T), Brunt-Vaisala frequency squared (N^2), vertical velocity (W), and the mixing ratios of cloud water (QCLOUD), graupel (QGRAUP), snow (QSNOW) and rain (QRAIN), for the reference period (2015–2035) (left) and future change (future period 2080–2100) (ssp370) (right). The vertical coordinate is height above sea level (m). The graphs in the bottom two panels display seasonal total precipitation (P) (left) and it's change (right). The sections are latitudinally averaged over the black box shown in the horizontal map at the bottom (the map is showing DJF total precipitation change as in Figure 5e).

of condensation shifting vertically upward over a mountains windward slope (Kirshbaum & Smith, 2008), causing the precipitation distribution to shift downstream (Siller & Roe, 2014), and the lower precipitation efficiency of warm cloud processes, lowering the precipitation response to below Clausius-Clapeyron scaling (Kirshbaum & Smith, 2008; Sandvik et al., 2018). Due to the general cooling of the region from the extreme NAWH we hypothesize that these warming effects are not particularly prominent in our results. To isolate the effects of the individual hypothesized mechanisms, and to more clearly separate the effects imposed by the NAWH from general global warming and circulation changes, it would be beneficial to perform a sensitivity study with idealized simulations.

Gervais et al. (2020) found contrasting responses in precipitation in relation to the NAWH through changes in jet regimes and surface heat fluxes, with the former producing a relatively weak increase where the enhanced jet hit the European coast, and the latter producing strong suppression of precipitation over the NAWH relatively constantly among their sensitivity experiments. This agrees well with our results. The stratiform component, which is mostly associated with low pressure systems, their fronts, and import of moisture from sources away from the sink region, shows increases where storms are projected to hit coastal Northern Europe more frequently (south of ~65°N). Convective precipitation on the other hand, is more strongly affected by changes in underlying surface heat and moisture fluxes. Papritz and Sodemann (2018) showed that up to 90% of the moisture taken up from the Nordic seas' surface during MCAO events falls as local precipitation through convective overturning (increasing values approaching the Norwegian west coast). This supports the strong impact of the SST cooling, and consequently reduced MCAOs, evaporation, and increased atmospheric static stability, on convective precipitation. We hypothesize that this contributes to both reduced convective triggering and convective intensity. The decrease in convective precipitation is robust across all the applied scenarios here, and exceeds the precipitation increase associated with increased moisture transport from storms to the south in the domain, and hence dominates the total precipitation change signal. Consequently, the dominant effect on future precipitation change in this region seems to be the underlying surface heat flux impact brought upon by the extreme NAWH.

Gervais et al. (2020) also point out that the spatial extent of the precipitation suppression and hence its possible impact on coastal Europe is highly dependent on the NAWH strength, spatial extent and location, which again is dependent on the slowdown of the AMOC. Both the AMOC and NAWH show a substantial spread among the CMIP5 and CMIP6 models (Bellomo et al., 2021; Hand et al., 2019), highlighting the large uncertainty involved in these future projections.

5. Summary and Conclusions

We summarize the main results from the WRF downscaling of CESM2 (member r11) with the ssp370 scenario and 12 km grid spacing. The changes are for 2080–2100 with respect to 2015–2035:

- Winter precipitation totals decrease by 10%–30% over the Norwegian Sea and western and northern Norway, while increasing by 10%–20% over the southern North Sea, Denmark, eastern Norway and southern Sweden.
- Stratiform precipitation decreases (10%–30%) north of and increases (10%–30%) south of 45°N (also valid for its frequency), which corresponds well with CESM2's projected changes in storm-track activity. The results show that prevailing wind directions change from westerly to south-westerly, indicating changes in the orientation of storm tracks. A southwesterly path will to a large extent detour the warming hole and pick up moisture from a warmer ocean surface along the way.
- Convective precipitation decreases by 10%–40% over its primary area of occurrence, which constitutes major parts of the Norwegian Sea and Norway's west coast. The reduced SSTs of the NAWH lead to reduced evaporation and increased atmospheric static stability, which contributes to reduce available moisture, convective triggering, convective intensity, and hence convective precipitation amounts.
- Orographic precipitation shows a distinct pattern of decrease (10%–30%) above and increase (10%–50%) below roughly 500 m.a.s.l. on the western slopes of the Scandinavian mountains. The results and literature indicate that this is related to (a) increased static stability, causing increased terrain flow blocking, which moves the zone of orographic lift upstream, (b) reduced cross-barrier wind speed, (c) the higher frequency of rain versus snow in a warmer climate (rain has a higher fall velocity which leads to a shorter horizontal advection distance, hence making the precipitation fall out further upstream than if it consisted predominantly of snow) (Colle, 2004; Pavelsky et al., 2012).
- The precipitation signals are robust responses in the downscaling experiments across the three scenarios (ssp126, ssp245, and ssp370). The responses are also evident in the CESM2 fields directly, and are also robust

across the range of scenarios and different ensemble members, although not with the same magnitude and level of detail as simulated with WRF.

To conclude, our results indicate that the anomalously cold SSTs of the NAWH as projected by CESM2 lead to a considerable decrease in winter convective precipitation in the region. The results further indicate that the local, direct negative surface heat and moisture flux impact of the NAWH on the convective precipitation dominates the impact of other global warming related aspects, including increased storm activity causing increased horizontal moisture transport and stratiform precipitation south of 45°N. The upstream shift in orographic precipitation distribution seems also to be, at least partly, connected to the NAWH through the increased static stability and flow blocking, however research is needed to isolate the individual proposed mechanisms. It should be stressed that our experiments are based on an extreme projection of the NAWH from one climate model and an end of the century period, serving as an extreme scenario, and that generally there are large uncertainties involved in climate model projections of the AMOC/NAWH. Nevertheless, this study contributes with evidence that there is a risk of substantial future decreases in winter precipitation over large parts of Scandinavia. Given the significant societal impacts of such changes, more research is urgently needed to constrain future climate projections in the North Atlantic region.

Data Availability Statement

The CMIP6 CESM2 data is openly available from the ESGF server: https://esgf-node.llnl.gov/search/cmip6/. The data behind this research is generated with the freely available Weather Research and Forecast (WRF) model (Skamarock et al., 2019) version 4.1.2. As noted, modifications have been made to one of the parameterization schemes of the model (the Thompson and Eidhammer microphysics scheme), which is documented in Iversen et al. (2021). The modified code is openly available (Emiliecive, 2021). The algorithm to separate out convective precipitation is based on Poujol et al. (2020), with the modifications listed in Supporting Information S1.

Acknowledgments

The authors would like to thank Statnett for enabling this research through the research project ICEBOX, funded by the Norwegian Research Council (NFR 282403). We acknowledge 321954 - FME NorthWind: Norwegian Research Centre on Wind Energy, KeyCLIM (NFR 295046), Sigma2: the National Infrastructure for High Performance Computing and Data Storage in Norway (computation from Nortur (NN9188K) and storage resources on NIRD (NS9816K and NS9252K)), the World Climate Research Programme, which, through its Working Group on Coupled Modelling, coordinated and promoted CMIP6. We thank the climate modeling groups for producing and making available their model output, the Earth System Grid Federation (ESGF) for archiving the data and providing access, and the multiple funding agencies who support CMIP6 and ESGF. The authors are also grateful for discussions with coworkers Kristian Ingvaldsen, Maria Sand, Oskar Landgren, Bjørg Jenny Kokkvoll Engdahl, and the main author is grateful for supervision by Trude Storelvmo.

References

Barnett, T. P., Pierce, D. W., Hidalgo, H. G., Bonfils, C., Santer, B. D., Das, T., et al. (2008). Human-induced changes in the hydrology of the western United States. *Science*, *319*(5866), 1080–1083. https://doi.org/10.1126/science.1152538

Bellomo, K., Angeloni, M., Corti, S., & von Hardenberg, J. (2021). Future climate change shaped by inter-model differences in Atlantic meridional overturning circulation response. *Nature Communications*, *12*(1), 3659. https://doi.org/10.1038/s41467-021-24015-w

Berg, P., Moseley, C., & Haerter, J. O. (2013). Strong increase in convective precipitation in response to higher temperatures. *Nature Geoscience*, *6*(3), 181–185. https://doi.org/10.1038/ngeo1731

Birch, C. E., Roberts, M. J., Garcia-Carreras, L., Ackerley, D., Reeder, M. J., Lock, A. P., & Schiemann, R. (2015). Sea-breeze dynamics and convection initiation: The influence of convective parameterization in weather and climate model biases. *Journal of Climate*, *28*(20), 8093–8108. https://doi.org/10.1175/jcli-d-14-00850.1

Brayshaw, D. J., Hoskins, B., & Blackburn, M. (2008). The storm-track response to idealized SST perturbations in an aquaplanet GCM. *Journal of the Atmospheric Sciences*, *65*(9), 2842–2860. https://doi.org/10.1175/2008jas2657.1

Bresson, H., Hodges, K. I., Shaffrey, L. C., Zappa, G., & Schiemann, R. (2022). The response of northern hemisphere polar lows to climate change in a 25 km high-resolution global climate model. *Journal of Geophysical Research: Atmospheres*, *127*(4), e2021JD035610. https://doi.org/10.1029/2021JD035610

Brümmer, B. (1997). Boundary layer mass, water, and heat budgets in wintertime cold-air outbreaks from the Arctic sea ice. *Monthly Weather Review*, *125*(8), 1824–1837. https://doi.org/10.1175/1520-0493(1997)125<1824:Blmwah>2.0.Co;2

Brümmer, B. (1999). Roll and cell convection in wintertime Arctic cold-air outbreaks. *Journal of the Atmospheric Sciences*, *56*(15), 2613–2636. https://doi.org/10.1175/1520-0469(1999)056<2613:Racciw>2.0.Co;2

Catto, J. L., Jakob, C., Berry, G., & Nicholls, N. (2012). Relating global precipitation to atmospheric fronts. *Geophysical Research Letters*, *39*(10), L10805. https://doi.org/10.1029/2012GL051736

Chernokulsky, A., Kozlov, F., Zolina, O., Bulygina, O., Mokhov, I. I., & Semenov, V. A. (2019). Observed changes in convective and stratiform precipitation in Northern Eurasia over the last five decades. *Environmental Research Letters*, *14*(4), 045001. https://doi.org/10.1088/1748-9326/aafb82

Cohen, J., Zhang, X., Francis, J. E. A., Jung, T., Kwok, R., Overland, J., et al. (2020). Divergent consensuses on Arctic amplification influence on midlatitude severe winter weather. *Nature Climate Change*, *10*(1), 20–29. https://doi.org/10.1038/s41558-019-0662-y

Colle, B. A. (2004). Sensitivity of orographic precipitation to changing ambient conditions and terrain geometries: An idealized modeling perspective. *Journal of the Atmospheric Sciences*, *61*(5), 588–606. https://doi.org/10.1175/1520-0469(2004)061<0588:Sooptc>2.0.Co;2

Danabasoglu, G., Lamarque, J.-F., Bacmeister, J., Bailey, D. A., DuVivier, A. K., Edwards, J., et al. (2020). The community Earth system model version 2 (CESM2). *Journal of Advances in Modeling Earth Systems*, *12*(2), e2019MS001916. https://doi.org/10.1029/2019MS001916

Dirmeyer, P. A., Cash, B. A., Kinter, J. L., Jung, T., Marx, L., Satoh, M., et al. (2012). Simulating the diurnal cycle of rainfall in global climate models: Resolution versus parameterization. *Climate Dynamics*, *39*(1), 399–418. https://doi.org/10.1007/s00382-011-1127-9

Drijfhout, S., van Oldenborgh, G. J., & Cimatoribus, A. (2012). Is a decline of AMOC causing the warming hole above the North Atlantic in observed and modeled warming patterns? *Journal of Climate*, *29*, 2359–2373.

Emiliecive (2021). *melting_snow* Version 1.0. Zenodo. https://doi.org/10.5281/zenodo.5707580

Field, P. R., Brožková, R., Chen, M., Dudhia, J., Lac, C., Hara, T., et al. (2017). Exploring the convective grey zone with regional simulations of a cold air outbreak. *Quarterly Journal of the Royal Meteorological Society*, *143*(707), 2537–2555. https://doi.org/10.1002/qj.3105

Gervais, M., Shaman, J., & Kushnir, Y. (2019). Impacts of the North Atlantic warming hole in future climate projections: Mean atmospheric circulation and the North Atlantic Jet. *Journal of Climate*, *32*(10), 2673–2689. https://doi.org/10.1175/jcli-d-18-0647.1

Gervais, M., Shaman, J., & Kushnir, Y. (2020). Impact of the North Atlantic warming hole on sensible weather. *Journal of Climate*, *33*(10), 4255–4271. https://doi.org/10.1175/jcli-d-19-0636.1

Graff, L. S., & LaCasce, J. H. (2012). Changes in the extratropical storm tracks in response to changes in SST in an AGCM. *Journal of Climate*, *25*(6), 1854–1870. https://doi.org/10.1175/jcli-d-11-00174.1

Han, X., Xue, H., Zhao, C., & Lu, D. (2016). The roles of convective and stratiform precipitation in the observed precipitation trends in Northwest China during 1961–2000. *Atmospheric Research*, *169*, 139–146. https://doi.org/10.1016/j.atmosres.2015.10.001

Hand, R., Keenlyside, N., Omrani, N.-E., & Latif, M. (2014). Simulated response to inter-annual SST variations in the Gulf Stream region. *Climate Dynamics*, *42*(3), 715–731. https://doi.org/10.1007/s00382-013-1715-y

Hand, R., Keenlyside, N. S., Omrani, N.-E., Bader, J., & Greatbatch, R. J. (2019). The role of local sea surface temperature pattern changes in shaping climate change in the North Atlantic sector. *Climate Dynamics*, *52*(1), 417–438. https://doi.org/10.1007/s00382-018-4151-1

Hohenegger, C., Brockhaus, P., & Schar, C. (2008). Towards climate simulations at cloud-resolving scales. *Meteorologische Zeitschrift*, *17*(4), 383–394. https://doi.org/10.1127/0941-2948/2008/0303

Hohenegger, C., Schlemmer, L., & Silvers, L. (2015). Coupling of convection and circulation at various resolutions. *Tellus A: Dynamic Meteorology and Oceanography*, *67*(1), 26678. https://doi.org/10.3402/tellusa.v67.26678

Houze, R. A. (2014). Chapter 6 - Nimbostratus and the separation of convective and stratiform precipitation. In R. A. Houze (Ed.), *International geophysics* (Vol. 104, pp. 141–163). Academic Press. https://doi.org/10.1016/B978-0-12-374266-7.00006-8

Hughes, M., Hall, A., & Fovell, R. G. (2009). Blocking in areas of complex topography, and its influence on rainfall distribution. *Journal of the Atmospheric Sciences*, *66*(2), 508–518. https://doi.org/10.1175/2008jas2689.1

Iacono, M. J., Delamere, J. S., Mlawer, E. J., Shephard, M. W., Clough, S. A., & Collins, W. D. (2008). Radiative forcing by long-lived greenhouse gases: Calculations with the AER radiative transfer models. *Journal of Geophysical Research*, *113*(D13), D13103. https://doi.org/10.1029/2008jd009944

Inatsu, M., Mukougawa, H., & Xie, S.-P. (2003). Atmospheric response to zonal variations in midlatitude SST: Transient and stationary eddies and their feedback. *Journal of Climate*, *16*(20), 3314–3329. https://doi.org/10.1175/1520-0442(2003)016<3314:artzvi>2.0.co;2

Iversen, E. C., Nygaard, B. E., Hodnebrog, Ø., Sand, M., & Ingvaldsen, K. (2023). Future projections of atmospheric icing in Norway. *Cold Regions Science and Technology*, *210*, 103836. https://doi.org/10.1016/j.coldregions.2023.103836

Iversen, E. C., Thompson, G., & Nygaard, B. E. (2021). Improvements to melting snow behavior in a bulk microphysics scheme. *Atmospheric Research*, *253*, 105471. https://doi.org/10.1016/j.atmosres.2021.105471

Jackson, L. C., Kahana, R., Graham, T., Ringer, M. A., Woollings, T., Mecking, J. V., & Wood, R. A. (2015). Global and European climate impacts of a slowdown of the AMOC in a high resolution GCM. *Climate Dynamics*, *45*(11), 3299–3316. https://doi.org/10.1007/s00382-015-2540-2

Kay, J. E., Deser, C., Phillips, A., Mai, A., Hannay, C., Strand, G., et al. (2015). The community Earth system model (CESM) large ensemble project: A community resource for studying climate change in the presence of internal climate variability. *Bulletin of the American Meteorological Society*, *96*(8), 1333–1349. https://doi.org/10.1175/bams-d-13-00255.1

Keil, P., Mauritsen, T., Jungclaus, J., Hedemann, C., Olonscheck, D., & Ghosh, R. (2020). Multiple drivers of the North Atlantic warming hole. *Nature Climate Change*, *10*(7), 667–671. https://doi.org/10.1038/s41558-020-0819-8

Kendon, E. J., Roberts, N. M., Fosser, G., Martin, G. M., Lock, A. P., Murphy, J. M., et al. (2020). Greater future U.K. winter precipitation increase in new convection-permitting scenarios. *Journal of Climate*, *33*(17), 7303–7318. https://doi.org/10.1175/jcli-d-20-0089.1

Kirshbaum, D. J., Adler, B., Kalthoff, N., Barthlott, C., & Serafin, S. (2018). Moist orographic convection: Physical mechanisms and links to surface-exchange processes. *Atmosphere*, *9*(3), 80. https://doi.org/10.3390/atmos9030080

Kirshbaum, D. J., & Smith, R. B. (2008). Temperature and moist-stability effects on midlatitude orographic precipitation. *Quarterly Journal of the Royal Meteorological Society*, *134*(634), 1183–1199. https://doi.org/10.1002/qj.274

Kolstad, E. W., & Bracegirdle, T. J. (2008). Marine cold-air outbreaks in the future: An assessment of IPCC AR4 model results for the northern hemisphere. *Climate Dynamics*, *30*(7), 871–885. https://doi.org/10.1007/s00382-007-0331-0

Kolstad, E. W., Bracegirdle, T. J., & Seierstad, I. A. (2009). Marine cold-air outbreaks in the North Atlantic: Temporal distribution and associations with large-scale atmospheric circulation. *Climate Dynamics*, *33*(2), 187–197. https://doi.org/10.1007/s00382-008-0431-5

Landgren, O. A., Seierstad, I. A., & Iversen, T. (2019). Projected future changes in marine cold-air outbreaks associated with polar lows in the Northern North-Atlantic Ocean. *Climate Dynamics*, *53*(5), 2573–2585. https://doi.org/10.1007/s00382-019-04642-2

Lavers, D. A., & Villarini, G. (2013). The nexus between atmospheric rivers and extreme precipitation across Europe. *Geophysical Research Letters*, *40*(12), 3259–3264. https://doi.org/10.1002/grl.50636

Lebeaupin, C., Ducrocq, V., & Giordani, H. (2006). Sensitivity of torrential rain events to the sea surface temperature based on high-resolution numerical forecasts. *Journal of Geophysical Research*, *111*(D12), D12110. https://doi.org/10.1029/2005jd006541

Lepore, C., Abernathey, R., Henderson, N., Allen, J. T., & Tippett, M. K. (2021). Future global convective environments in CMIP6 models. *Earth's Future*, *9*(12), e2021EF002277. https://doi.org/10.1029/2021EF002277

Li, Y., Li, Z., Zhang, Z., Chen, L., Kurkute, S., Scaff, L., & Pan, X. (2019). High-resolution regional climate modeling and projection over western Canada using a weather research forecasting model with a pseudo-global warming approach. *Hydrology and Earth System Sciences*, *23*(11), 4635–4659. https://doi.org/10.5194/hess-23-4635-2019

Liu, W., Fedorov, A. V., Xie, S.-P., & Hu, S. (2020). Climate impacts of a weakened Atlantic meridional overturning circulation in a warming climate. *Science Advances*, *6*(26), eaaz4876. https://doi.org/10.1126/sciadv.aaz4876

Luce, C. H., Abatzoglou, J. T., & Holden, Z. A. (2013). The missing mountain water: Slower westerlies decrease orographic enhancement in the Pacific Northwest USA. *Science*, *342*(6164), 1360–1364. https://doi.org/10.1126/science.1242335

Mallet, P.-E., Claud, C., & Vicomte, M. (2017). North Atlantic polar lows and weather regimes: Do current links persist in a warmer climate? *Atmospheric Science Letters*, *18*(8), 349–355. https://doi.org/10.1002/asl.763

Mitchell, K. (2005). The community noah land-surface model (LSM).

Nakamura, H., Sampe, T., Tanimoto, Y., & Shimpo, A. (2004). Observed associations among storm tracks, jet streams and midlatitude oceanic fronts. *Earth's Climate: The Ocean–Atmosphere Interaction, Geophys. Monogr*, *147*, 329–345.

Nakanishi, M., & Niino, H. (2006). An improved Mellor–Yamada level-3 model: Its numerical stability and application to a regional prediction of advection fog. *Boundary-Layer Meteorology*, *119*(2), 397–407. https://doi.org/10.1007/s10546-005-9030-8

O'Neill, B. C., Tebaldi, C., van Vuuren, D. P., Eyring, V., Friedlingstein, P., Hurtt, G., et al. (2016). The scenario model Intercomparison project (ScenarioMIP) for CMIP6. *Geoscientific Model Development*, *9*(9), 3461–3482. https://doi.org/10.5194/gmd-9-3461-2016

Oudar, T., Cattiaux, J., & Douville, H. (2020). Drivers of the northern extratropical eddy-driven jet change in CMIP5 and CMIP6 models. *Geophysical Research Letters*, *47*(8), e2019GL086695. https://doi.org/10.1029/2019gl086695

Panziera, L., & Germann, U. (2010). The relation between airflow and orographic precipitation on the southern side of the Alps as revealed by weather radar. *Quarterly Journal of the Royal Meteorological Society*, *136*(646), 222–238. https://doi.org/10.1002/qj.544
Papritz, L., & Grams, C. M. (2018). Linking low-frequency large-scale circulation patterns to cold air outbreak formation in the northeastern North Atlantic. *Geophysical Research Letters*, *45*(5), 2542–2553. https://doi.org/10.1002/2017GL076921
Papritz, L., & Sodemann, H. (2018). Characterizing the local and intense water cycle during a cold air outbreak in the Nordic Seas. *Monthly Weather Review*, *146*(11), 3567–3588. https://doi.org/10.1175/mwr-d-18-0172.1
Papritz, L., & Spengler, T. (2017). A Lagrangian climatology of wintertime cold air outbreaks in the Irminger and Nordic seas and their role in shaping air–sea heat fluxes. *Journal of Climate*, *30*(8), 2717–2737. https://doi.org/10.1175/jcli-d-16-0605.1
Pavelsky, T. M., Sobolowski, S., Kapnick, S. B., & Barnes, J. B. (2012). Changes in orographic precipitation patterns caused by a shift from snow to rain. *Geophysical Research Letters*, *39*(18), L18706. https://doi.org/10.1029/2012GL052741
Pearson, K. J., Lister, G. M. S., Birch, C. E., Allan, R. P., Hogan, R. J., & Woolnough, S. J. (2014). Modelling the diurnal cycle of tropical convection across the 'grey zone'. *Quarterly Journal of the Royal Meteorological Society*, *140*(679), 491–499. https://doi.org/10.1002/qj.2145
Poujol, B., Mooney, P. A., & Sobolowski, S. P. (2021). Physical processes driving intensification of future precipitation in the mid- to high latitudes. *Environmental Research Letters*, *16*(3), 034051. https://doi.org/10.1088/1748-9326/abdd5b
Poujol, B., Sobolowski, S., Mooney, P., & Berthou, S. (2020). A physically based precipitation separation algorithm for convection-permitting models over complex topography. *Quarterly Journal of the Royal Meteorological Society*, *146*(727), 748–761. https://doi.org/10.1002/qj.3706
Prein, A. F., Langhans, W., Fosser, G., Ferrone, A., Ban, N., Goergen, K., et al. (2015). A review on regional convection-permitting climate modeling: Demonstrations, prospects, and challenges. *Reviews of Geophysics*, *53*(2), 323–361. https://doi.org/10.1002/2014RG000475
Purnell, D. J., & Kirshbaum, D. J. (2018). Synoptic control over orographic precipitation distributions during the Olympics Mountains Experiment (OLYMPEX). *Monthly Weather Review*, *146*(4), 1023–1044. https://doi.org/10.1175/mwr-d-17-0267.1
Rulfová, Z., & Kyselý, J. (2013). Disaggregating convective and stratiform precipitation from station weather data. *Atmospheric Research*, *134*, 100–115. https://doi.org/10.1016/j.atmosres.2013.07.015
Sandvik, I. M., Sorteberg, A., & Rasmussen, R. (2018). Sensitivity of historical orographically enhanced extreme precipitation events to idealized temperature perturbations. *Climate Dynamics*, *50*(1–2), 143–157. https://doi.org/10.1007/s00382-017-3593-1
Screen, J. A., Bracegirdle, T. J., & Simmonds, I. (2018). Polar climate change as manifest in atmospheric circulation. *Current Climate Change Reports*, *4*(4), 383–395. https://doi.org/10.1007/s40641-018-0111-4
Shaw, T. A., Baldwin, M., Barnes, E. A., Caballero, R., Garfinkel, C. I., Hwang, Y. T., et al. (2016). Storm track processes and the opposing influences of climate change. *Nature Geoscience*, *9*(9), 656–664. https://doi.org/10.1038/ngeo2783
Siller, N., & Roe, G. (2014). How will orographic precipitation respond to surface warming? An idealized thermodynamic perspective. *Geophysical Research Letters*, *41*(7), 2606–2613. https://doi.org/10.1002/2013gl059095
Skamarock, W. C., Klemp, J. B., Dudhia, J., Gill, D. O., Liu, Z., Berner, J., et al. (2019). A description of the advanced research WRF version 4.
Smith, R. B. (1989). Hydrostatic airflow over mountains. In B. Saltzman (Ed.), *Advances in geophysics* (Vol. 31, pp. 1–41). Elsevier. https://doi.org/10.1016/S0065-2687(08)60052-7
Smith, R. B., & Barstad, I. (2004). A linear theory of orographic precipitation. *Journal of the Atmospheric Sciences*, *61*(12), 1377–1391. https://doi.org/10.1175/1520-0469(2004)061<1377:Altoop>2.0.Co;2
Stein, T. H., Parker, D. J., Hogan, R. J., Birch, C. E., Holloway, C. E., Lister, G. M., et al. (2015). The representation of the West African monsoon vertical cloud structure in the met office unified model: An evaluation with CloudSat. *Quarterly Journal of the Royal Meteorological Society*, *141*(693), 3312–3324. https://doi.org/10.1002/qj.2614
Stohl, A., Forster, C., & Sodemann, H. (2008). Remote sources of water vapor forming precipitation on the Norwegian west coast at 60°N–a tale of hurricanes and an atmospheric river. *Journal of Geophysical Research*, *113*(D5), D05102. https://doi.org/10.1029/2007JD009006
Swingedouw, D., Bily, A., Esquerdo, C., Borchert, L. F., Sgubin, G., Mignot, J., & Menary, M. (2021). On the risk of abrupt changes in the North Atlantic subpolar gyre in CMIP6 models. *Annals of the New York Academy of Sciences*, *1504*(1), 187–201. https://doi.org/10.1111/nyas.14659
Tang, S., Gleckler, P., Xie, S., Lee, J., Ahn, M.-S., Covey, C., & Zhang, C. (2021). Evaluating the diurnal and semidiurnal cycle of precipitation in CMIP6 models using satellite- and ground-based observations. *Journal of Climate*, *34*(8), 3189–3210. https://doi.org/10.1175/jcli-d-20-0639.1
Thompson, G., & Eidhammer, T. (2014). A study of aerosol impacts on clouds and precipitation development in a large winter cyclone. *Journal of the Atmospheric Sciences*, *71*(10), 3636–3658. https://doi.org/10.1175/jas-d-13-0305.1
Tomassini, L., Field, P. R., Honnert, R., Malardel, S., McTaggart-Cowan, R., Saitou, K., et al. (2017). The "Grey Zone" cold air outbreak global model intercomparison: A cross evaluation using large-eddy simulations. *Journal of Advances in Modeling Earth Systems*, *9*(1), 39–64. https://doi.org/10.1002/2016MS000822
Trenberth, K. E. (1999). Atmospheric moisture recycling: Role of advection and local evaporation. *Journal of Climate*, *12*(5), 1368–1381. https://doi.org/10.1175/1520-0442(1999)012<1368:Amrroa>2.0.Co;2
Trenberth, K. E., Dai, A., Rasmussen, R. M., & Parsons, D. B. (2003). The changing character of precipitation. *Bulletin of the American Meteorological Society*, *84*(9), 1205–1218. https://doi.org/10.1175/bams-84-9-1205
Vellinga, M., Roberts, M., Vidale, P. L., Mizielinski, M. S., Demory, M.-E., Schiemann, R., et al. (2016). Sahel decadal rainfall variability and the role of model horizontal resolution. *Geophysical Research Letters*, *43*(1), 326–333. https://doi.org/10.1002/2015GL066690
Vergara-Temprado, J., Ban, N., Panosetti, D., Schlemmer, L., & Schär, C. (2020). Climate models permit convection at much coarser resolutions than previously considered. *Journal of Climate*, *33*(5), 1915–1933. https://doi.org/10.1175/jcli-d-19-0286.1
Wilcox, E. M., & Donner, L. J. (2007). The frequency of extreme rain events in satellite rain-rate estimates and an atmospheric general circulation model. *Journal of Climate*, *20*(1), 53–69. https://doi.org/10.1175/jcli3987.1
Wilson, C., Sinha, B., & Williams, R. G. (2009). The effect of ocean dynamics and orography on atmospheric storm tracks. *Journal of Climate*, *22*(13), 3689–3702. https://doi.org/10.1175/2009jcli2651.1
Woollings, T., Gregory, J., Pinto, J., Reyers, M., & Brayshaw, D. (2012). Response of the North Atlantic storm track to climate change shaped by ocean–atmosphere coupling. *Nature Geoscience*, *5*, 313–317. https://doi.org/10.1038/ngeo1438
Woollings, T., Harvey, B., Zahn, M., & Shaffrey, L. (2012). On the role of the ocean in projected atmospheric stability changes in the Atlantic polar low region. *Geophysical Research Letters*, *39*(24), L24802. https://doi.org/10.1029/2012gl054016
Zahn, M., & von Storch, H. (2010). Decreased frequency of North Atlantic polar lows associated with future climate warming. *Nature*, *467*(7313), 309–312. https://doi.org/10.1038/nature09388
Zappa, G., & Shepherd, T. G. (2017). Storylines of atmospheric circulation change for European regional climate impact assessment. *Journal of Climate*, *30*(16), 6561–6577. https://doi.org/10.1175/jcli-d-16-0807.1